Post-print version:

Providing frequency support to offshore energy hubs using hydrogen and wind reserves

H. Pozo Gonzalez, F.D. Bianchi, N.A. Cutululis, J.L. Dominguez-Garcia

BibTex:

Providing frequency support to offshore energy hubs using hydrogen and wind reserves

Hector del Pozo Gonzalez[a,*], Fernando D. Bianchi[b,c], Nicolaos A. Cutululis[d] and
Jose Luis Dominguez-Garcia[a]

[a]*Catalonia Institute for Energy Research (IREC), Jardins de les Dones de Negre, 08930, Sant Adrià de Besòs, Barcelona, Spain*

[b]*Instituto Tecnológico Buenos Aires (ITBA), Ciudad Autónoma de Buenos Aires, Argentina*

[c]*Consejo Nacional de Investigaciones Científicas y Técnicas (CONICET), Ciudad Autónoma de Buenos Aires, Argentina*

[d]*Department of Wind Energy, Technical University of Denmark (DTU), 4000 Roskilde, Denmark*

ABSTRACT

This paper presents a case study of an offshore energy hub integrating two wind farms, potential HVDC connections to multiple countries, and hydrogen production facilities. The analysis focuses on the capacity to provide frequency support using reserves from wind and electrolyzer plants located in different parts of the network. The study also analyzes the trade-off in terms of economic profit between renewable energy sales and the cost of maintaining a power reserve for the provision of frequency support. An attractive feature of using electrolyzers and wind farms for frequency support is that their power contributions are opposite; the former adsorbs power and the latter injects power and vice versa. This is used to improve the overall economic profit. Nevertheless, time responses of each kind of plant are different and this might affect the primary frequency support. Simulation results indicate that a proper management of wind and hydrogen reserves may allow an effective compromise, ensuring a satisfactory primary frequency control.

Nomenclature

$\bar{x}$	The bar over the variable denotes value at the operating point
$\hat{x}$	The hat over the variable denotes incremental value w.r.t $\bar{x}$
f	Electrical frequency
P_{dc}	DC power adsorbed or injected into the MT-HVDC
P_g	AC mechanical power
P_{hy}	Power converted into hydrogen
P_{ld}	AC power demand
P_r	AC mechanical power set-point
P_w	Power delivered by the WPP
P_w^{av}	Available wind power
R^+, R^-	Upward and downward total power reserves
R_{hy}^+, R_{hy}^-	Upward and downward electrolyzer power reserves
R_w^+, R_w^-	Upward and downward wind power reserves
V_{dc}	DC voltage

*Corresponding author:
✉ hdelpozo@irec.cat (H. del Pozo Gonzalez)
ORCID(s): 0000-0002-4270-1353 (H. del Pozo Gonzalez);
0000-0001-7332-6501 (F.D. Bianchi); 0000-0003-2438-1429 (N.A. Cutululis);
0000-0002-0483-995X (J. Dominguez-Garcia)

1. Introduction

Offshore energy islands represent a significant step toward the development of future offshore energy hubs. An offshore energy hub is defined as a fully renewable combination of assets, which links offshore generation, interconnection, and some type of storage [1]. The Bornholm project is a good example of these energy hubs, which aims to become a pioneering Danish energy hub by 2030 [2]. The project involves the construction of a full-scale offshore energy hub by 2050 [3]. The most probable current locations for these hubs are areas in the North Sea and in the Baltic Sea [4].

The study of energy hubs has been addressed from industry and academia perspectives. A preliminary electrical infrastructure about the Bornholm project can be found in [2, 5]. This planned energy hub includes two offshore wind farms, a high-voltage direct current (HVDC) converter station, and transmission cables connecting the wind plants, the converter station, and energy consumers in Zealand, Denmark. The plan also involves potential interconnections with Germany and Poland in the future. The electrical infrastructure aspects of the Bornholm project, such as the capacity of the wind farm, the layouts, and the cable configurations, along with the considerations of the power quality, are studied in the report [5]. More recently, the Energinet report [6] analyzed the cable system requirements of the Bornholm hub from a market perspective. Koivisto et al. [7] investigated the system-wide effects of offshore energy hubs in the Baltic Sea, concluding that the largest and most cost-effective deployment of these hubs by 2050 will occur in a highly electrified system, particularly in the southern region. On the other hand, Luth et al. [8, 9] focused on the use of

electrolysis to improve the system flexibility. Similar studies can be found for the North Sea application [10, 11, 12].

Although the concept of offshore energy islands is emerging as a topic of considerable interest, most studies focus mainly on implementation aspects. The experience in close research areas suggests that these energy islands might participate in the provision of ancillary services. For example, some studies have shown that offshore wind farms can support frequency regulation in AC networks through multi-terminal HVDC systems, using both centralized [13, 14] and decentralized approaches [15, 16]. Studies, such as [17, 18], have investigated multi-area-based systems and developed algorithms for frequency support, which could also serve as a basis.

The use of hydrogen reserves might also contribute to the frequency support. Although this topic has not been extensively explored, some works show promising findings. For instance, in [19, 20, 21], the response of different low-temperature grid-connected electrolysis technologies has been analyzed, along with the potential advantages they may offer in the delivery of ancillary services. Similar studies have also been conducted for high-temperature grid-connected electrolysis technologies [22, 23].Other studies, such as [24, 25], which highlight the potential of hydrogen to support the grid while enhancing profitability through participation in secondary markets such as the natural gas and emerging hydrogen markets.

As can be seen, some studies have examined frequency support in interconnected areas from offshore wind and the low-power use of electrolyzers. However, there is still a research gap in the integrated modeling and analysis of offshore energy hubs combining large-scale wind and hydrogen. To the best of our knowledge, it has not yet been studied how coordinated reserve management of wind and hydrogen can simultaneously support the grid and deliver economic benefits. Therefore, taking into account the potential of energy hubs for the provision of frequency support, this paper presents the following key contributions:

- The proposal of a hypothetical study case of an offshore energy hub that integrates a hybrid multiterminal HVDC (MT-HVDC) system with wind farms, electrolysis stations and AC areas.

- A hierarchical control strategy to provide frequency support in the AC areas using the power reserve available in the wind and hydrogen plants. The strategy includes an upper level control aimed to estimate the most suitable power reserve levels in hydrogen and wind plants based on the economic cost of the energy sales and the provision of ancillary services.

This article is structured as follows. First, Section 2 presents the concept and definition of the offshore energy hub, along with its control-oriented modeling. Section 3 outlines a control strategies for primary frequency support and for the optimization of the power reserve levels considering the total economic profit. Section 4 presents a

Figure 1: Schematic representation of the multi-terminal HVDC offshore energy island system under study, connecting two wind farms, three AC areas, and two electrolyzer plants.

thorough evaluation of the proposed control strategy and, finally, Section 5 concludes with the main findings.

2. Control-oriented model for the energy island system

2.1. Concept and system definition

Figure 1 presents the system under study, which consists of three AC areas, two offshore wind farms, and two electrolyzer plants. The three AC areas are assumed to be located in three geographically separated areas. There is an energy island that serves as a hub to concentrate the power distribution between the offshore wind farms and the AC areas. One of the electrolyzer plants is located close to AC area 1 and the other on the energy island (Station 6), simulating offshore hydrogen production. These components are connected to each other through voltage source converters (VSCs) within a multi-terminal HVDC (MT-HVDC) network. The demand in the AC areas is met by the power delivered from a conventional power plant and by the power absorbed from the MT-HVDC grid.

The main purpose of this system is to utilize the power generated by the wind farms to meet a part of the consumption in the AC areas and to produce green hydrogen, which is stored in local tanks or injected into a gas network. The objective here is to study the capability of wind farms and electrolyzer plants to provide frequency support in AC areas. In particular, their capability to momentarily increase or decrease the power supplied to the AC areas to compensate for power imbalances and restore their electrical frequencies.

To design a frequency control strategy, each station in the system shown in Figure 1 is modeled following the approach introduced in [14, 16].

2.2. AC area modeling

AC areas are approximated by a single aggregated synchronous generator with a frequency-dependent load [26]. Therefore, the dynamics of the AC area j connected to

Station i is assumed governed by:

$$\frac{df_j}{dt} = \frac{P_{g,j} - P_{ld,j} - P_{dc,i}}{4\pi^2 f_{nom} J_j}$$
$$- \left(\frac{P_{ld,j} D_{ld,j}}{4\pi^2 f_{nom} J_j} + \frac{D_{g,j}}{J_j} \right)(f_j - f_{nom}), \quad (1)$$

$$\frac{dP_{g,j}}{dt} = \frac{1}{\tau_{g,j}}(P_{r,j} - P_{g,j}), \quad i = j = 1, 2, 3, \quad (2)$$

where f_j is the electrical frequency, f_{nom} is the nominal frequency, J_j and $D_{g,j}$ are the inertia and the generator damping, respectively, $D_{ld,j}$ is the load damping, $P_{g,j}$ is the mechanical power, and $P_{ld,j}$ is the power demand in the area. The DC power demanded from the multi-terminal network through Station i is $P_{dc,i}$. Equation (2) describes the behavior of the speed governor in the synchronous generator with $\tau_{g,j}$ a time-constant and $P_{r,j}$ a set-point.

Let us define the following incremental variables:

$$\hat{f}_j = f_j - f_{nom}, \qquad \hat{P}_{g,j} = P_{g,j} - \bar{P}_{g,j} \quad (3)$$
$$\hat{P}_{dc,i} = P_{dc,i} - \bar{P}_{dc,i}, \qquad \hat{P}_{ld,j} = P_{ld,j} - \bar{P}_{ld,j}, \quad (4)$$
$$\hat{P}_{r,j} = P_{r,j} - \bar{P}_{r,j}, \quad (5)$$

with the bar over the variables denoting the operating point values at which the model is linearized. Hence, the linearized model can be described by:

$$\frac{d\hat{f}_j}{dt} = -a_{1,j}\hat{f}_j + a_{2,j}(\hat{P}_{g,j} - \hat{P}_{ld,j} - \hat{P}_{dc,i}), \quad (6)$$

$$\frac{d\hat{P}_{g,j}}{dt} = -a_{3,j}\hat{P}_{r,j} + a_{3,j}\hat{P}_{g,j}, \quad (7)$$

with $a_{1,j} = (D_{g,j} + \bar{P}_{ld,j} D_{ld,j}/(4\pi^2 f_{nom}))/J_j$, $a_{2,j} = 1/(4\pi^2 f_{nom} J_j)$, and $a_{3,j} = 1/\tau_{g,j}$.

2.3. Wind farm and electrolyzer modeling

For control design purposes, wind farms are modeled as power sources that aggregate the power contributions of all turbines on the farm. Hence, the total power generated by the equivalent wind turbine is given by:

$$P_{w,l} = \kappa_l C_P(\Omega_l, W_l, \theta_l) W_l^3, \quad l = 1, 2, \quad (8)$$

where κ_l is a constant, $C_P(\cdot)$ the power coefficient, W_l an average wind speed, Ω_l the shaft speed, and θ_l the blade pitch angle. The last two variables are used to control the power generated by the aggregate wind turbine.

On the other hand, the electrolyzers are modeled as power sources absorbing power to produce hydrogen that is injected into a gas network. Therefore, there are no limits in the absorbed energy, but there exist lower and upper limits in the power as discussed in Section 3.1.3.

2.4. MT-HVDC grid modeling

The MT-HVDC grid is assumed to be a resistive electrical network, as a consequence, at each Station i the relation between the voltage and power is described by

$$P_{dc,i} = V_{dc,i} \sum_{k=1}^{7} \frac{V_{dc,i} - V_{dc,k}}{R_{ik}}, \quad i = 1, \dots, 7, \quad (9)$$

where R_{ik} is the resistance of the cable connecting Station i and k and $V_{dc,i}$ the voltage at the node i. In case there is no link between node i and k, the resistance R_{ik} is assumed to be infinite.

Defining the incremental variables $\hat{V}_{dc,i} = V_{dc,i} - V_{nom}$ and linearizing (9), the small-signal model results

$$\hat{P}_{dc,i} = \frac{\bar{P}_{dc,i}}{V_{nom}} \hat{V}_{dc,i} + V_{nom} \sum_{k=1}^{7} \frac{\hat{V}_{dc,i} - \hat{V}_{dc,k}}{R_{ik}}, \quad (10)$$

with $i = 1, \dots, 7$ and V_{nom} the nominal DC voltage.

3. Frequency support control strategy

We proposed a control strategy based on the results introduced in [14, 16]. The strategy consists of four control levels:

1. *Local power controls* at each station: the automatic generator control (AGC) in the AC areas, the power generation control in the wind farms, and the hydrogen production control.
2. A droop *DC voltage control* that ensures power transmission under normal conditions.
3. *An automatic and distributed primary frequency control* aimed to coordinate the power contributions of the wind and hydrogen plants to restore the frequency in the AC areas after changes in the power demand.
4. *A supervisory control* with the purpose of setting the long-term power generation of wind and hydrogen plants in order to maximize the economic profit of selling wind energy, hydrogen, and maintaining a certain level of power reserve.
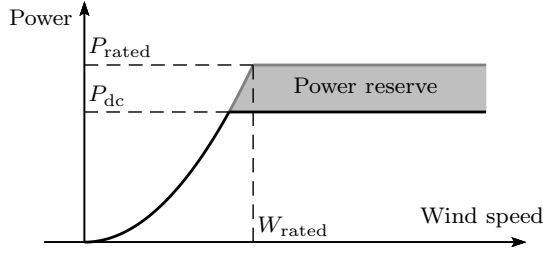
3.1. Local power controls
3.1.1. Local frequency control at AC areas

Each AC area j, connected to the MT-HVDC through Station i, includes an AGC with the aim of restoring a medium-term power balance. This control law is given by:

$$\hat{P}_{r,j} = -K_{fp,j}\hat{f}_j + K_{Pi,j} \int \hat{P}_{dc,i} dt, \quad j = i = 1, 2, 3, \quad (11)$$

where $K_{fp,j} = \bar{P}_{g,j}/\sigma_j f_{nom}$, and $K_{Pi,j}$ a parameter to be designed. This control law is intended to compensate for frequency droops without contributions from the MT-HVDC grid. The last term in (11) ensures that, in medium-term, the conventional generator compensates for the power imbalance and thus the power reserve in the wind farms is restored.

Figure 2: De-loading power control strategy used in the wind farms

3.1.2. Wind farm local control

The power generation in the wind farms follows a de-loading strategy as shown in Figure 2. The farm control ensures that the power supplied by the wind plant is kept at a set-point $P_{dc,i}$ as long as this value is between a lower limit $P_{w,l}^{min}$ and the available wind power $P_{w,l}^{av}$ given by

$$P_{w,l}^{av} = \begin{cases} \kappa_l C_{P,max} W_l^3, & \text{if } W_l < W_{rated,l}, \\ P_{rated,l}, & \text{otherwise,} \end{cases} \quad l = 1, 2, \quad (12)$$

where $C_{P,max}$ is the maximum value of the power coefficient, and W_{rated} the rated wind speed. The set-point $P_{dc,i}$ is the DC power delivered to the MT-HVDC network through Station i ($i = l + 3$). Therefore, maintaining the set-point within these limits allows the wind farm to keep a power reserve to provide frequency support to the AC areas.

3.1.3. Electrolyzer control

In each electrolyzer, it is assumed that a control strategy ensures that a power $P_{dc,i}$ is absorbed from the MT-HVDC network through Station i with dynamic responses governed by a time-constant $\tau_{hy,m}$. That is:

$$\frac{dP_{hy,m}}{dt} = \frac{1}{\tau_{hy,m}}(P_{rh,m} - P_{hy,m}), \quad m = 1, 2, \quad (13)$$

where $P_{hy,m}$ the electrical power converted into hydrogen and $P_{rh,m}$ a set-point. The choice of the time-constant $\tau_{hy,m}$ is based on the experimental response times of PEM electrolyzers in fast frequency support in other similar works [27]. These set-points are assumed bounded according to:

$$P_{rh,m} = \begin{cases} P_{hy,m}^{min} & \text{if } P_{dc,i} < P_{hy,m}^{min}, \\ P_{h,m}^{max} & \text{if } P_{dc,i} > P_{hy,m}^{max}, \\ P_{dc,i}, & \text{otherwise,} \end{cases}$$

with $i = m + 5$, $P_{hy,m}^{min}$ and $P_{hy,m}^{max}$ the lower and upper power limits, respectively. The power limits of the hydrogen system are primarily determined by the need for electrolyzers to operate within specific cell voltage ranges to ensure optimal performance, prevent degradation, and maintain efficient hydrogen production. Acceptable voltage levels vary by electrolyzer type and operational conditions. As an example, between the main typologies, alkaline electrolyzers require

a minimum voltage of 1.5 to 1.8 volts and a maximum of 2.0 to 2.5 volts; proton exchange membrane (PEM) electrolyzers operate between 1.6 to 2.0 volts minimum and 2.0 to 2.5 volts maximum; while solid oxide electrolyzers (SOEC) function within a range of 1.2 to 1.5 volts minimum and 1.8 to 2.5 volts maximum [28, 29, 30]. However, for the sake of simplicity and given the large size of the electrolysis plants, we have used these values exclusively to define the minimum power limits for the entire plant, irrespective of the specific technology employed.

3.2. Droop DC voltage control

With the aim of ensuring the desired power transmission under normal conditions, the strategy includes a DC voltage droop control. That is, a decentralized control law given by:

$$\hat{P}_{dc,V,i} = -K_{Vp,i}\hat{V}_{dc,i}, \quad i = 1, 2, 3, \quad (14)$$

where $K_{Vp,i} = \bar{P}_{g,i}/V_{nom}$. This control is only implemented in the AC areas.

3.3. Automatic primary frequency control

To provide automatic frequency support in the AC areas, the contribution of the wind farms and electrolyzers are coordinated with a distributed control strategy. This strategy consists of three different control laws for the AC areas, for the wind farms, and for the electrolyzer plants. In the AC areas, the control law is given by

$$\hat{P}_{dc,f,i} = \alpha \int \hat{f}_j \, dt + \beta \hat{f}_j, \quad i = j = 1, 2, 3, \quad (15)$$

where α and β are parameters tuned as discussed in [16].

In the wind farms, the control law is given by

$$\hat{P}_{dc,w,i} = \begin{cases} \hat{P}_{w,l}^{min}, & \text{if } w_l < \hat{P}_{w,l}^{min} \\ w_l, & \text{if } \hat{P}_{w,l}^{min} \le w_l \le \hat{P}_{w,l}^{max}, \\ \hat{P}_{w,l}^{max} & \text{if } \hat{P}_{w,l}^{max} > w_l \end{cases} \quad (16)$$

where $l = 1, 2$, $i = l + 3$, and

$$w_l = \sum_{j=1}^{3} \phi_{l,j} \left(\alpha \int \hat{f}_j \, dt + \beta \hat{f}_j \right). \quad (17)$$

The limits $\hat{P}_{w,l}^{min}$ and $\hat{P}_{w,l}^{max}$ are imposed by the available wind resources $P_{w,l}^{av}$. The additional weights $\phi_{l,j}$ serve to prioritize the frequency regulation in the area j. In electrolyzers, a control law similar to (16) is used to produce the control input $\hat{P}_{dc,hy,i}$, $i = 6, 7$.

To sum up, the control at each station is

$$\hat{P}_{dc,i} = \begin{cases} \hat{P}_{dc,f,i} + \hat{P}_{dc,V,i}, & i = 1, 2, 3, \\ \hat{P}_{dc,w,i}, & i = 4, 5, \\ \hat{P}_{dc,hy,i}, & i = 6, 7. \end{cases} \quad (18)$$

In case of an increase in consumption in an AC area j, the corresponding station transmits the effect on its electrical

frequency f_j with the aim that the wind farms and the electrolyzers change the power injected to and absorbed from, respectively, the MT-HVDC network. This increases the power $P_{\text{dc},i}$ and restores the frequency f_j. In the medium-term, local control (11) increases $P_{\text{g},j}$ to ensure that the power contributions from the wind farms and electrolyzers return to the values prior to the frequency disturbance event, and thus they are able to restore the total power reserve available in the system.

3.4. Supervisory control

The ability of the lower control levels to compensate for frequency deviations in AC areas depends on the power reserves in the wind farms and electrolyzers. With this aim, wind farms and electrolyzers should operate below their rated power generation. This implies a reduction in the profit from the sale of wind energy and hydrogen.

The power reserve is determined by the set-points $\bar{P}_{\text{dc},i}$. In case of wind farms ($i = 4, 5$ and $l = i - 3$):

$$R_{\text{w},l}^{+} = P_{\text{w},l}^{\text{av}} - \bar{P}_{\text{dc},i}, \tag{19}$$

$$R_{\text{w},l}^{-} = \bar{P}_{\text{dc},i} - P_{\text{w},l}^{\text{min}}, \tag{20}$$

and in case of electrolyzers ($i = 6, 7$ and $m = i - 5$):

$$R_{\text{hy},m}^{+} = \bar{P}_{\text{dc},i} - P_{\text{hy},m}^{\text{min}}, \tag{21}$$

$$R_{\text{hy},m}^{-} = P_{\text{hy},m}^{\text{max}} - \bar{P}_{\text{dc},i}, \tag{22}$$

where the superscripts $^{+}$ and $^{-}$ stand for upward and downward power reserves, respectively. The total upward and downward power reserves result:

$$R^{+} = \sum_{l=1}^{2} R_{\text{w},l}^{+} + \sum_{m=1}^{2} R_{\text{hy},m}^{+}, \tag{23}$$

$$R^{-} = \sum_{l=1}^{2} R_{\text{w},l}^{-} + \sum_{m=1}^{2} R_{\text{hy},m}^{-}. \tag{24}$$

Notice that wind farms and electrolyzers provide opposite contributions to power reserves. Thus, without sacrificing the energy profit, this scheme ensures minimum values of reserves:

$$R_{\text{min}}^{+} = \sum_{m=1}^{2} P_{\text{hy},m}^{\text{max}} - P_{\text{hy},m}^{\text{min}}, \tag{25}$$

$$R_{\text{min}}^{-} = \sum_{l=1}^{2} P_{\text{w},l}^{\text{av}} - P_{\text{w},l}^{\text{min}}. \tag{26}$$

In order to maximize the system capability for providing frequency support, the DC power set-points are updated every hour based on the forecasting for the energy prices, the consumes, and the available wind power. These set-points are determined by solving the following optimization problem:

$$\underset{\bar{\mathbf{P}}_g, \bar{\mathbf{P}}_{\text{dc}}}{\text{maximize}} \sum_{t=k}^{k+N-1} J(\mathbf{C}_{\text{r}}, \mathbf{C}_{\text{e},j}, \mathbf{C}_{\text{hy}}, \bar{\mathbf{P}}_g, \bar{\mathbf{P}}_{\text{dc}}, \mathbf{R}^{+}, \mathbf{R}^{-}, t)$$

subject to

$$
\begin{aligned}
0 &= \bar{P}_{\text{ld},j} - \bar{P}_{\text{g},j} - \bar{P}_{\text{dc},i}, & i = j = 1, 2, 3, \\
0 &= \sum_{i=1}^{7} \bar{P}_{\text{dc},i}, & R^{+} \geq \varepsilon_2, \\
P_{\text{g},j} &\geq 0, \ \bar{P}_{\text{dc},i} \geq \varepsilon_1, & i = j = 1, 2, 3, \\
P_{\text{w},l}^{\text{min}} &\leq \bar{P}_{\text{dc},i} \leq P_{\text{w},l}^{\text{av}}, & l = 1, 2, \ i = l + 3, \\
P_{\text{hy}}^{\text{min}} &= \bar{P}_{\text{dc},i} \leq P_{\text{hy}}^{\text{max}}, & i = 6, 7,
\end{aligned}
\tag{27}
$$

where

$$\bar{\mathbf{P}}_{\ell} = \begin{bmatrix} \bar{P}_{\ell,1}(k) & \cdots & \bar{P}_{\ell,1}(k+N) \\ \bar{P}_{\ell,2}(k) & \cdots & \bar{P}_{\ell,2}(k+N) \\ \bar{P}_{\ell,3}(k) & \cdots & \bar{P}_{\ell,3}(k+N) \end{bmatrix}, \quad \ell \in \{\text{g}, \text{dc}\}. \tag{28}$$

The objective function is defined as

$$J(\mathbf{C}_{\text{r}}, \mathbf{C}_{\text{e},j}, \mathbf{C}_{\text{hy}}, \bar{\mathbf{P}}_g, \bar{\mathbf{P}}_{\text{dc}}, \mathbf{R}^{+}, \mathbf{R}^{-}, t) = \underbrace{\mathbf{C}_{\text{hy}}(t) \sum_{i=6}^{7} \bar{P}_{\text{dc},i}(t)}_{\text{Hydrogen profit}}$$

$$+ \underbrace{\mathbf{C}_{\text{r}}(t) \sum_{l=1}^{2} R_{\text{w},l}^{+}}_{\text{Reserve profit}} + \underbrace{\sum_{j=1}^{3} \mathbf{C}_{\text{e},j}(t) \bar{P}_{\text{dc},j}(t)}_{\text{Wind energy profit}} + \varepsilon_1 + \varepsilon_2, \tag{29}$$

where $\mathbf{C}_{\text{r}}(k, N)$, $\mathbf{C}_{\text{e},j}(k, N)$, $\mathbf{C}_{\text{hy}}(k, N)$ are the price fore-casting vectors for the reserve, the electrical energy at each AC area j, and the hydrogen, respectively, from the instant k and with an horizon of N samples (e.g. $\mathbf{C}_{\text{r}}(k, N) = [C_{\text{r}}(k), \ldots, C_{\text{r}}(k + N)]$). The subscript $j = 1, 2, 3$ in the energy price corresponds to the price forecast for AC areas 1, 2 and 3, respectively. The sampling time will be set at one hour and $N = 24$. The aim is to maximize the profit for maintaining a power reserve and selling wind energy and hydrogen.

4. Results

The control strategy proposed for the case study presented in Figure 1 was evaluated using Matlab/Simulink, and Yalmip [31] and Mosek [32] to solve the optimization problem (27). The parameters corresponding to the dynamics of the system areas, DC transmission lines, wind farms, and electrolyzers are listed in Table 1. These values have been adapted for the present case study from [33, 3, 2]. Wind farms are represented as aggregate turbines with a scaled two-mass model of the NREL benchmark turbine [34], with a standard PI local control to track the power references

Table 1
Parameters corresponding to the power system under study

AC area j	1	2	3
J_j (kgm^2)	147726.29	984841.91	218853.76
$D_{g,j}$ (kWs^2)	60.79	81.06	60.79
$D_{ld,j}$ (s)	0.08	0.10	0.08
$\tau_{g,j}$ (s)	6.00	8.00	6.00
$K_{fp,j}$ (MW/Hz)	800.55	1108.96	799.99
σ_j (s)	0.05	0.15	0.07
$\bar{P}_{r,j}$ (GW)	1.82	8.17	2.70
$\bar{P}_{ld,j}$ (GW)	2.23	9.72	3.37
$\bar{P}_{dc,i}$ (GW) ($i = j$)	−0.40	−1.55	−0.67
Line resistances	$R_{17} = 3.97\,\Omega$	$R_{27} = 2.47\,\Omega$	$R_{37} = 3.80\,\Omega$
	$R_{47} = 0.19\,\Omega$	$R_{57} = 0.19\,\Omega$	$R_{16} = 0.02\,\Omega$
Wind farm l		1	2
Max Power (GW)		1.41	2.39
$\bar{P}_{dc,i}$ (GW) ($i = l + 3$)		1.27	2.15
Electrolyzer m		1	2
Max Power (GW)		0.50	0.30
$\bar{P}_{dc,i}$ (GW) ($i = m + 5$)		−0.45	−0.27
$\tau_{h,m}$ (s)		0.1	0.1

described in Section 3.1.2. The nominal DC voltage in the MT-HVDC network is $V_{nom} = 525$ kV [6]. The VSCs are modeled as a current source controlled by power and a capacitor. Considering the difference in the time frames for the primary frequency control level and the supervisory control responsible for the power reserve management, both controls are evaluated in different simulation scenarios.

4.1. Primary frequency control

The automatic primary frequency control is evaluated in multiple scenarios. The first two scenarios analyze the frequency support when the available wind power is high. The last scenarios consider situations where the upward power reserve in the wind farm is low. Before any disturbance, the DC powers $\bar{P}_{dc,i}$, the AC loads $\bar{P}_{ld,j}$, and the AC power set-points $\bar{P}_{r,j}$ correspond to the values listed in Table 1. In steady-state conditions, the wind farm and electrolyzer powers coincide with the DC power absorbed or injected through the corresponding station.

4.1.1. High available wind power

Figure 3 presents simulation results in the event that an increase of 137 MW occurs in AC area 1 (Station 1). This implies a negative step of 137 MW in $\hat{P}_{ld,1}$ at the instant 25 s as shown in Figure 3c. In this case, the wind power upward reserves are assumed to be $R_{w,1}^+ = 141$ MW and $R_{w,2}^+ = 239$ MW, and the electrolyzer upward reserves are $R_{hy,1}^+ = 450$ MW and $R_{hy,2}^+ = 270$ MW. Figure 3b shows the incremental DC power $\hat{P}_{dc,i}$ for each station. As a result of the frequency control, Station 1 increases the power absorbed from the MT-HVDC network to balance demand in the AC area and transmits frequency disturbance to Stations 4 to 7. In this scenario, both wind farms have a sufficient power reserve to contribute to frequency support and provide fast contributions $\hat{P}_{dc,4}$ and $\hat{P}_{dc,5}$. On the other hand,
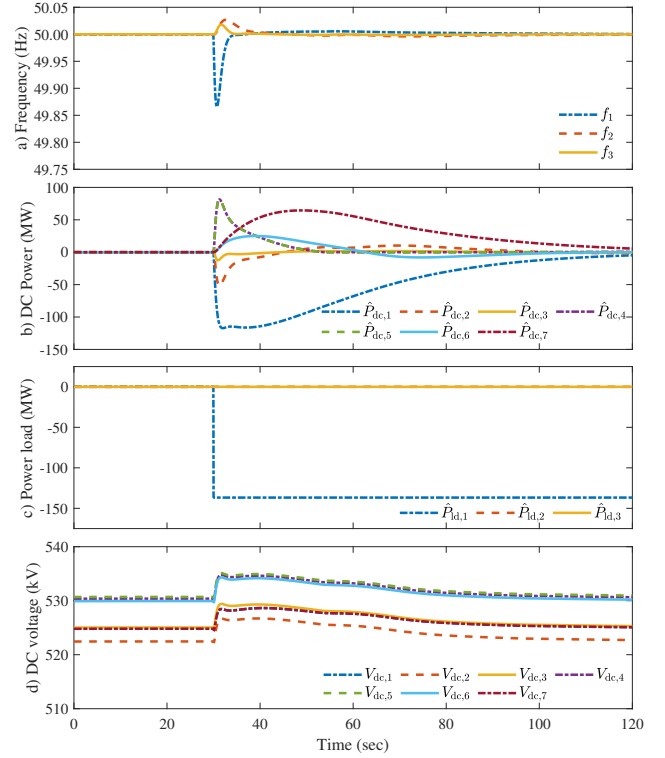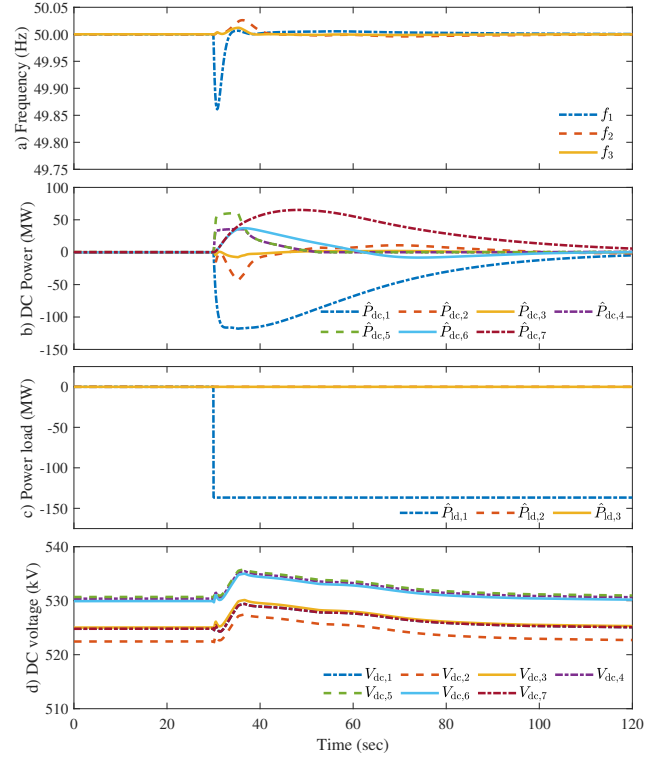

Figure 3: Primary frequency control: closed-loop response for an increase of 137 MW in the power demand in AC area 1 when the available wind power is high

electrolyzers reduce the power extracted from MT-HVDC grids, implying an increase in incremental values $\hat{P}_{dc,6}$ and $\hat{P}_{dc,7}$. In this case, the electrolyzer located closer to Station 1, provides the highest contribution. Note also that the wind farms are able to provide a faster compensation than the electrolyzer nodes. Finally, Figure 3d presents the voltage at each node. As a consequence of the droop control (14) and the changes in power contributions, the voltages at every node are disturbed and this causes small perturbations in the frequencies of the other AC areas. It should be noted that, after the initial frequency compensation, the power absorbed by Station 1 gradually decreases until it reaches zero. This behavior is produced by the local power control law (11), which increases AC generation and thereby progressively restores the total power reserve.

The closed-loop response corresponding to a load disturbance of 152 MW in AC area 2 can be seen in Figure 4. The power reserves are assumed to be the same as in the previous scenario. In this case, the initial wind power contributions are similar to the previous scenario. However, the power contribution $\hat{P}_{dc,7}$ from electrolyzer in Station 7 is significantly smaller as this station is too distant from the AC area 2. Consequently, the rest of the stations must increase their power contributions. In particular, it can be observed that, to properly reject the frequency disturbance, the wind farms must maintain the additional power contribution for a longer period of time and the other electrolyzer must also reduce the power absorbed (i.e. an increase of $\hat{P}_{dc,6}$). As
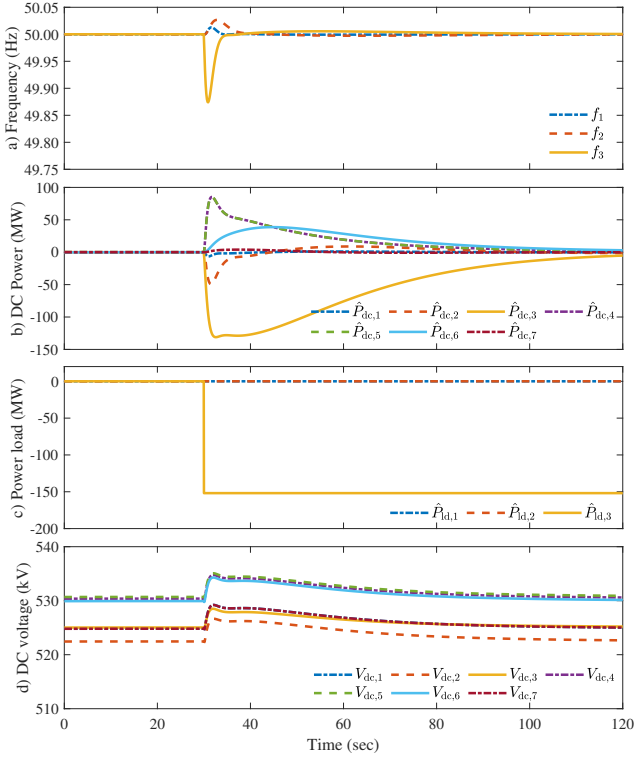
Figure 4: Primary frequency control: closed-loop response for an increase of 152 MW in the power demand in AC area 2 when the available wind power is high

Figure 5: Primary frequency control: closed-loop response for an increase of 137 MW in the power demand in AC area 1 when the available wind power is low

in the other scenario, the AGC (11) gradually increases the local generation and the power reserve returns to the original values.

4.1.2. Low available wind power

Figure 5 shows simulation results for a scenario similar to the one in Figure 3, i.e., an increase of 137 MW in the power demand in AC area 1. However, in this case, the available wind power is 75% lower. That is, the wind power upward reserves are $R_{w,1}^+ = 35.25$ MW and $R_{w,2}^+ = 59.70$ MW. The electrolyser reserves remain unchanged. As can be seen, the contribution of wind farms saturates and the electrolyzer plants must provide higher power contributions to compensate for the frequency error. Also note that this error compensation takes longer as the electrolyzer power responses are slower.

Figure 6 presents the closed-loop response for a scenario analogous to that analyzed in Figure 4, but with the same lower power reserves than the case of Figure 5. In contrast to the situation illustrated in Figure 4, the system exhibits a slower response to load disturbances due to the saturation of the wind farms, as indicated by the green and purple signals in Figure 6b. Unfortunately, the responses of the hydrogen stations are not sufficiently rapid to effectively restore the system frequency as in the case presented in Figure 4.

In both cases, the corresponding AGCs gradually increase the power set-points $\hat{P}_{r,j}$ in order to replenish the total power reserve available for primary frequency support.
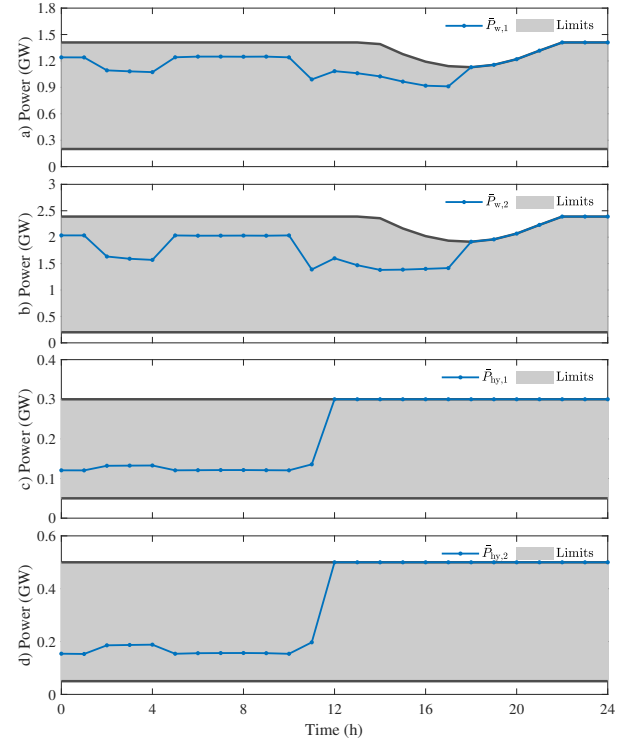
4.2. Power reserve optimization

Figures 7 to 9 present an example response of the supervisory control level aimed to optimize the total power reserve proposed in Section 3.4. The energy prices for the three AC areas, the hydrogen sale and the reserve are shown in Figure 7a. The price for maintaining a power reserve is assumed to remain constant at 100 €/MWh over the optimization horizon. The available wind powers and the electrolyzer limits are plotted in Figure 8 with black lines. The energy prices and power demand profiles are inspired by real data from [35]. To emphasize the behavior of the algorithm, the remaining prices and profiles have been adapted to construct a sufficiently rich scenario.

The resulting total power reserves R^+ and R^- can be seen in Figure 7b. The power set-points $\bar{P}_{dc,i}$ corresponding to the wind farms and the electrolyzers can be seen in Figure 8. Figure 9 shows the power balances in each AC area. The black lines correspond to the AC power demand $P_{ld,j}$, the light yellow areas to the power generated in the AC area, and the light blue areas to the power absorbed from the MT-HVDC network. It can be observed that the algorithm prioritizes the wind power delivering to the AC areas when the energy prices are higher, especially in AC area 3 that has the highest energy price. As a result, the power reserve is lower in the period of time of higher prices. Notice that, after the 12-th hour, the hydrogen prices rise and therefore the hydrogen production also increases. When energy prices rise after the 17-th hour, the algorithm maximizes the wind
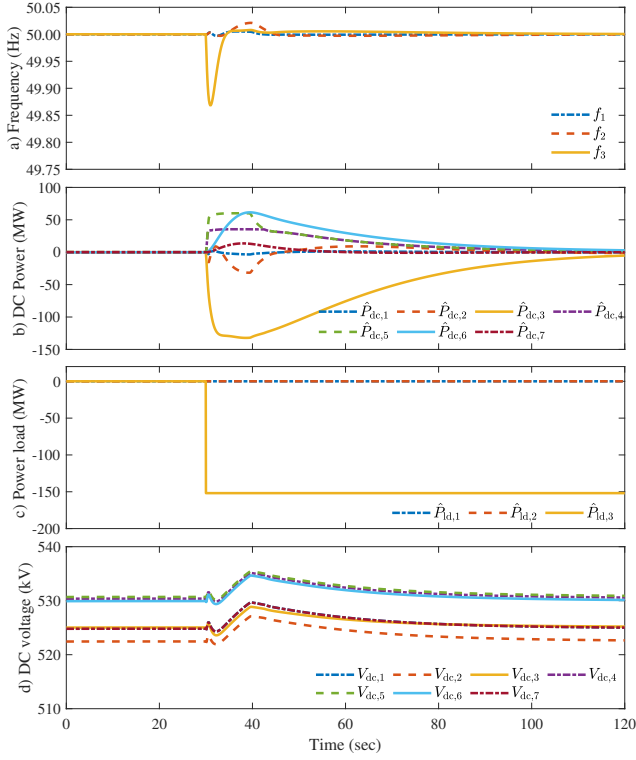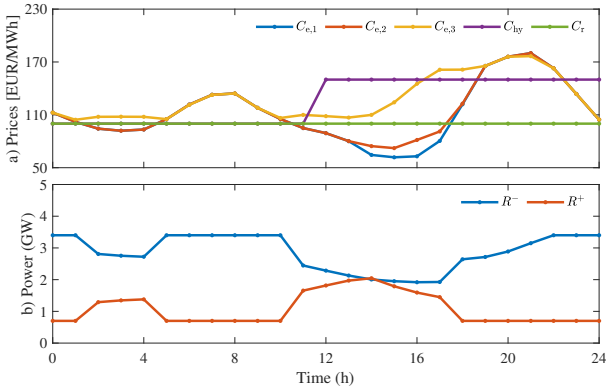
Figure 6: Primary frequency control: closed-loop response for an increase of 152 MW in the power demand in AC area 2 when the available wind power is low

Figure 8: Power reserve optimization example: power delivered to and absorbed from corresponding to Stations 4-7 and their limits
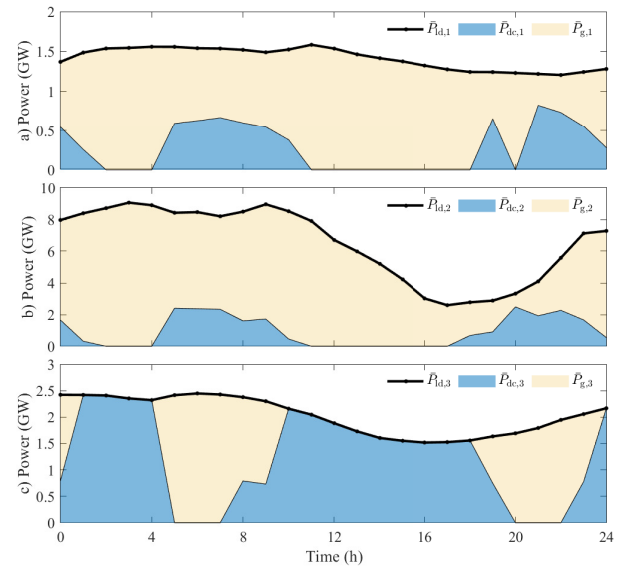

Figure 7: Power reserve optimization example: a) energy prices for each AC area, hydrogen production and reserve, b) upwards and downwards power reserves.

power delivered to the AC areas and the upward reserve falls to the minimum value, as this maximizes the overall profit.

Figure 9: Power reserve optimization example: Power balance at each AC area

5. Conclusions

This study of a hypothetical offshore energy hub shows that the integration of wind farms and electrolysis stations might effectively support primary frequency control through HVDC connections. By deploying wind farms alongside electrolysis plants, the hub leverages complementary response characteristics: wind farms enable rapid responses

for immediate frequency adjustments, whereas electrolyzers provide a stable but slower reserve capacity. However, the slower response time of electrolyzers limits their effectiveness in handling rapid frequency events. Optimizing reserve allocation between these technologies allows the hub to maintain system stability while maximizing economic

returns. Simulation results suggest that a well-balanced reserve strategy between wind and electrolysis plants can achieve satisfactory frequency control, allowing offshore hubs to effectively address the trade-off between renewable energy sales and the costs of maintaining reserve capacity, thereby supporting grid stability across interconnected areas.

Further work could focus on extending the proposed modeling and control strategies to provide frequency support in specific real-world scenarios. In particular, these methods could be adapted and applied to planned offshore energy hubs such as those in the North Sea and around the Bornholm Energy Island, where coordinated control of multiple assets will be essential to maintain interconnected hubs stability. In addition, further work could also analyze the capabilities of different electrolysis technologies for frequency support considering efficiency maximization, voltage constraints or idling effects during frequency restoration.

Acknowledgements

References

[1] Alexandra Lüth and Dogan Keles. Risks, strategies, and benefits of offshore energy hubs: A literature-based survey. *Renewable and Sustainable Energy Reviews*, 203:114761, 2024.

[2] Jacob Østergaard, Erik Damgaard Christensen, Kirsten Halsnæs, Christian Riisager-Simonsen, Dennis Lisbjerg, Anker Degn Jensen, Jens Øllgaard Duus, Henrik Madsen, Henrik Lund Frandsen, Mehdi Savaghebi, et al. Denmark as the energy island pioneer. Technical report, Technical University of Denmark, 2023.

[3] DNV. Screening of possible hub concepts to integrate offshore wind capacity in the north sea. Technical report, 2022.

[4] Philipp Glaum, Fabian Neumann, and Tom Brown. Offshore power and hydrogen networks for europe's north sea. *Applied Energy*, 369:123530, 2024.

[5] Energistyrelsen. Elektriske systemer for Bornholm I + II, Nordsøen II + III og Området vest for Nordsøen II + III: Finscreening af havarealer til etablering af nye havmølleparker med forbindelse til energiø/hub, May 2020. Project No. A132994, Document No. A132994-2-4.

[6] Energinet and 50Hertz Transmission GmbH. Bornholm energy island: Market dialogue on cables discussion paper. Technical report, Fredericia, Denmark and Berlin, Germany, 2023. Doc. 23/04783-2.

[7] M. Koivisto, P. Kanellas, R. Bramstoft, H. Koduvere, and J. P. Murcia Leon. Offshore energy hubs: cost-effectiveness in the Baltic sea energy system towards 2050. In *Proc. of 21st Wind & Solar Integration Workshop (WIW 2022)*, volume 2022, pages 24–29, 2022.

[8] Alexandra Lüth, Paul E Seifert, Ruud Egging-Bratseth, and Jens Weibezahn. How to connect energy islands: Trade-offs between hydrogen and electricity infrastructure. *Applied Energy*, 341:121045, 2023.

[9] Alexandra Lüth, Yannick Werner, Ruud Egging-Bratseth, and Jalal Kazempour. Electrolysis as a flexibility resource on energy islands: The case of the north sea. *Energy Policy*, 185:113921, 2024.

[10] Malte Jansen, Connor Duffy, Tim C Green, and Iain Staffell. Island in the sea: The prospects and impacts of an offshore wind power hub in the north sea. *Advances in Applied Energy*, 6:100090, 2022.

[11] Espen Flo Bødal, Sigmund Eggen Holm, Avinash Subramanian, Goran Durakovic, Dimitri Pinel, Lars Hellemo, Miguel Muñoz Ortiz, Brage Rugstad Knudsen, and Julian Straus. Hydrogen for harvesting the potential of offshore wind: A north sea case study. *Applied Energy*, 357:122484, 2024.

[12] Bernardo Castro Valerio, Vinicius A Lacerda, Marc Cheah-Mane, Pieter Gebraad, and Oriol Gomis-Bellmunt. An optimal power flow tool for ac/dc systems, applied to the analysis of the north sea grid for offshore wind integration. *IEEE Transactions on Power Systems*, 2025.

[13] Lingling Fan, Zhixin Miao, and Dale Osborn. Wind farms with HVDC delivery in load frequency control. *IEEE Transactions on Power Systems*, 24(4):1894–1895, 2009.

[14] Fernando D. Bianchi and Jose Luis Dominguez-Garcia. Coordinated frequency control using MT-HVDC grids with wind power plants. *IEEE Transactions on Sustainable Energy*, 7(1):213–220, January 2016.

[15] B Silva, CL Moreira, L Seca, Y Phulpin, and JA Pecas Lopes. Provision of inertial and primary frequency control services using offshore multiterminal HVDC networks. *IEEE Transactions on Sustainable Energy*, 3(4):800–808, 2012.

[16] Fernando D. Bianchi, Jose Luis Dominguez-Garcia, and Til Kristian Vrana. Distributed frequency control with partial information using MT-HVDC grids and WPPs. *IEEE Systems Journal*, 13(2):1694–1701, June 2019.

[17] Elyas Rakhshani, Daniel Remon, Antoni Mir Cantarellas, Jorge Martinez Garcia, and Pedro Rodriguez. Virtual synchronous power strategy for multiple HVDC interconnections of multi-area AGC power systems. *IEEE Transactions on Power Systems*, 32(3):1665–1677, 2016.

[18] Anne Mai Ersdal, Lars Imsland, and Kjetil Uhlen. Model predictive load-frequency control. *IEEE Transactions on Power Systems*, 31(1):777–785, 2015.

[19] Mehdi Ghazavi Dozein, Ahvand Jalali, and Pierluigi Mancarella. Fast frequency response from utility-scale hydrogen electrolyzers. *IEEE Transactions on Sustainable Energy*, 12(3):1707–1717, 2021.

[20] Chunjun Huang, Yi Zong, Shi You, and Chresten Træholt. Analytical modeling and control of grid-scale alkaline electrolyzer plant for frequency support in wind-dominated electricity-hydrogen systems. *IEEE Transactions on Sustainable Energy*, 14(1):217–232, 2022.

[21] Saman Dadjo Tavakoli, Mehdi Ghazavi Dozein, Vinícius A Lacerda, Marc Cheah Mañe, Eduardo Prieto-Araujo, Pierluigi Mancarella, and Oriol Gomis-Bellmunt. Grid-forming services from hydrogen electrolyzers. *IEEE Transactions on Sustainable Energy*, 14(4):2205–2219, 2023.

[22] Hector del Pozo Gonzalez, Lucile Bernadet, Marc Torrell, Fernando D Bianchi, Albert Tarancón, Oriol Gomis-Bellmunt, and Jose Luis Dominguez-Garcia. Power transition cycles of reversible solid oxide cells and its impacts on microgrids. *Applied Energy*, 352:121887, 2023.

[23] Hector del Pozo Gonzalez, Marc Torrell, Lucile Bernadet, Fernando D Bianchi, Lluís Trilla, Albert Tarancón, and Jose Luis Domínguez-García. Mathematical modeling and thermal control of a 1.5 kW reversible solid oxide stack for 24/7 hydrogen plants. *Mathematics*, 11(2):366, 2023.

[24] Nastaran Gholizadeh, Gevork B Gharehpetian, M Abedi, Hamed Nafisi, and Mousa Marzband. An innovative energy management framework for cooperative operation management of electricity and natural gas demands. *Energy Conversion and Management*, 200:112069, 2019.

[25] Hector del Pozo Gonzalez, Fernando D Bianchi, Marc Torrell, Lucile Bernadet, Josh Eichman, Albert Tarancón, Jose Luis Dominguez-Garcia, and Oriol Gomis-Bellmunt. Predictive control for mode-switching of reversible solid oxide cells in microgrids based on hydrogen and electricity markets. *International Journal of Hydrogen Energy*, 102:120–128, 2025.

[26] P. Kundur. *Power System Stability and Control*. McGraw-Hill, New York, USA, 1994.

[27] J Eichman and K Harrison. Novel electrolyzer applications: providing more than just hydrogen. Technical report, National Renewable

Energy Lab.(NREL), Golden, CO (United States), 2014.

[28] Mingyong Wang, Zhi Wang, Xuzhong Gong, and Zhancheng Guo. The intensification technologies to water electrolysis for hydrogen production–a review. *Renewable and sustainable energy reviews*, 29:573–588, 2014.

[29] Katherine Ayers. The potential of proton exchange membrane–based electrolysis technology. *Current Opinion in Electrochemistry*, 18:9–15, 2019.

[30] Kewei Hu, Jiakun Fang, Xiaomeng Ai, Danji Huang, Zhiyao Zhong, Xiaobo Yang, and Lei Wang. Comparative study of alkaline water electrolysis, proton exchange membrane water electrolysis and solid oxide electrolysis through multiphysics modeling. *Applied Energy*, 312:118788, 2022.

[31] Johan Lofberg. YALMIP: A toolbox for modeling and optimization in MATLAB. In *Proc. of the IEEE international conference on robotics and automation*, pages 284–289, 2004.

[32] MOSEK ApS. *The MOSEK optimization toolbox for MATLAB manual. Version 10.1.*, 2024.

[33] Cigré. Guide for the development of models for HVDC converters in a HVDC grid, 2015.

[34] J Jonkman. Definition of a 5-MW reference wind turbine for offshore system development. Technical report, National Renewable Energy Laboratory, 2009.

[35] Fraunhofer Institute for Solar Energy Systems ISE. Energy-Charts. https://energy-charts.info/index.html?l=en&c=DE, 2024. Accessed: 2024-08-04.